Structure of Tip Leakage Flow in a Forward-Swept Axial-Flow Fan Operating at Different Loading Conditions

Gong Hee Lee, Hwan Joo Myung*, Je-Hyun Baek†

Department of Mechanical Engineering, POSTECH, Pohang 790-784, Korea

**Digital Appliance Research Laboratory, LG Electronics, Seoul 153-023, Korea*

Key words: Axial-flow fan, Blade loading, LDV, Leakage vortex, Reynolds stress model, Tip clearance

ABSTRACT: An experimental analysis using three-dimensional Laser Doppler Velocimetry (LDV) measurement and computational analysis using the Reynolds stress model in FLUENT are conducted to give a clear understanding of the effect of blade loading on the structure of tip leakage flow in a forward-swept axial-flow fan operating at the maximum efficiency condition (ϕ=0.25) and two off-design conditions (ϕ=0.21 and 0.30). As the blade loading increases, the onset position of the rolling-up of tip leakage flow moves upstream and the trajectory of tip leakage vortex center is more inclined toward the circumferential direction. Because the casing boundary layer becomes thicker and the mixing between the through-flow and the leakage jet with the different flow direction is enforced, the streamwise vorticity decays more fast with the blade loading increasing. A distinct tip leakage vortex is observed downstream of the blade trailing edge at ϕ=0.30, but it is not observed at ϕ=0.21 and 0.25.

Nomenclature

C_{ps} : static pressure coefficient
C_x : axial chord length
D_c : casing diameter
D_h : hub diameter
L : shaft power
LE : leading edge
P : static pressure
PS : pressure side
Q : volume flow rate
R_{tip} : blade tip radius
SS : suction side
TE : trailing edge
TI : turbulence intensity
U_t : blade tip speed
$\vec{W}$: relative velocity vector
y^+ : dimensionless wall distance

Greek symbols

Ω : angular velocity
ϕ : flow coefficient
η : static efficiency
ρ : fluid density
$\vec{\omega}$: absolute vorticity vector
ω_s : streamwise vorticity
Ψ : static pressure rise coefficient

Subscripts

1 : inlet
s : streamwise direction
x : axial direction

† Corresponding author
Tel.: +82-54-279-2168; fax: +82-54-279-3199
E-mail address: jhbaek@postech.ac.kr

τ : normal direction

1. Introduction

As low speed axial-flow fans have been increasingly used in the various engineering applications, for examples, a room air-conditioner, a refrigerator, and a ventilator, the saving of power consumption via fan efficiency improvements emerges as an important issue. With the aim of obeying the environmental regulations and ensuring the market share, the reduction of noise level becomes another major goal in the fan design.

Tip leakage flow, which is driven by the pressure difference between the pressure and suction side of the blade tip, rolls up into a tip leakage vortex (TLV), which constitutes the dominant mechanisms of noise generation by an unsteady interaction with the fan blades (broadband noise) or the leading edge of the following blades (tonal noise).[1,2] The formation of TLV depends on various parameters, such as configuration of turbomachinery, tip clearance size, Mach number, annulus wall boundary layer, and blade loading. Among them, the blade loading is a major control parameter to give a direct influence on the onset position of TLV and its strength. Wagner et al.[3] found that the blockage due to the hub corner stall and tip leakage flow in the endwall regions increased rapidly with loading. Lakshminarayana and Pandya[4] acquired the pitchwise velocity field at various axial and radial locations between the compressor blade tip and the casing by using a hot-wire probe in combination with the ensemble-averaging techniques. They reported that the magnitudes of tip leakage flow were reduced with blade loading decreasing, and the nonintrusive measurement techniques were essential to investigate the roll-up of tip leakage flow. Myung and Baek[5] experimentally investigated the effect of tip leakage flow on the wake flow according to the loading conditions. They showed that the radially outward velocity increased and the position of its maximum value was close to the blade tip region with the loading increasing.

Unfortunately, most of the studies related with TLV were mainly confined to the industrial compressor and there has been little information available in open literature with regard to the detailed structure of TLV in an axial-flow fan. Even if the flow characteristics in an axial-flow fan are similar to those in a subsonic axial compressor, some geometric parameters, such as low hub-to-tip ratio, high stagger angle, and low solidity at the tip, are very different from the typical compressor geometry, so that an intensive study is required to find the peculiar flow characteristics in an axial-flow fan. In the current study, an experimental analysis using three-dimensional laser Doppler velocimetry (LDV) measurement and computational analysis using the Reynolds stress model of the commercial flow solver, FLUENT,[6] are conducted to give a clear understanding of the effect of blade loading on the structure of tip leakage flow in a forward-swept axial-flow fan. The results obtained from this study will help to develop the control techniques to suppress the detrimental effect of tip leakage flow in a low-speed axial-flow fan.

2. Experimental facility

Figure 1 shows a schematic view of a for-

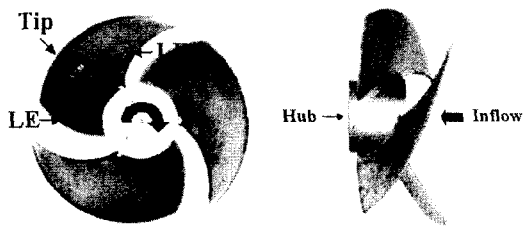

(a) Front view (b) Side view

Fig. 1 A schematic view of an axial-flow fan.

Table 1 Geometry specifications

Number of blade	3
Tip radius	113.5 mm
Hub radius	40.0 mm
Max. blade thickness	3.0 mm
Tip clearance size	5.0 mm
Blade type	Circular arc
Blade design	Free vortex
Rotational speed	1,500 rpm
Flow angle; outlet	60.5°
Sweep angle	42.5°

ward-swept axial-flow fan. It is usually attached to the electronics compartment of a refrigerator for cooling and defrosting. A blade is designed for the free vortex operation with the axial inflow condition. It has a circular-arc type camber line. By slightly rounding the suction side of the blade, blade thickness on the edges (i.e., leading, trailing, and tip edges) can be negligible. To reduce the noise generation due to the interaction of the inlet flow disturbance with the leading edge of the blade, the blade has a forward-sweep shape with 42.5° sweep angle. Tip clearance size is 5 mm, which corresponds to about 2.4% of tip chord length. Detailed geometric specifications of a test fan are given in Table 1.

The flow field is measured by the DANTEC three-dimensional laser Doppler velocimetry (LDV) system operating in the back-scattering mode. The statistical uncertainty of the radial velocity component can be lowered below 1.7% by a careful adjustment. The uncertainty of the axial and the circumferential velocity are lower than that of the radial velocity.

Measurement positions of tip leakage flow are denoted as '1' in Fig. 2. From 3 mm downstream of the blade leading edge, there are 21 traverse planes with 5 mm increment between the two adjacent planes at peak efficiency condition ($\phi=0.25$) and 11 planes with 10 mm space at large flow rate condition ($\phi=0.30$). At each traverse plane, there are 16 radial stations with

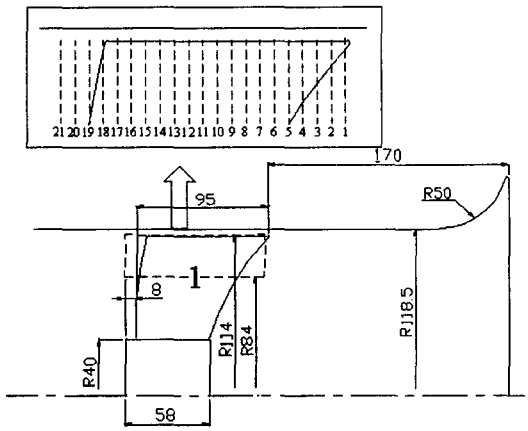

Fig. 2 Measurement positions (Dimension: mm).

2 mm increment from $r/R_{tip}=0.74$ to 1.004. Further discussions of the experimental facility, measurement technique, and error analysis can be found in the previous studies.[7-9]

3. Numerical method

The steady incompressible turbulent flow in an axial-flow fan is computed with the commercial flow solver, FLUENT.[6] The computation is conducted in the relative coordinate system rotating with the blade row. Due to the interaction of tip leakage flow with the through-flow and the casing boundary layer, the second-order accurate upwind differencing for the convection terms of each governing equation is used to minimize the cross-stream numerical diffusion. Convergence criterion requires that the scaled residuals decrease to 10^{-5} for all equations.

Since the RSM can take naturally into account the effect of rotation on turbulence, it is selected as the turbulence model in the present study. More detailed descriptions of the numerical scheme and boundary conditions can be found in Lee et al.[10]

Figure 3 shows the grid system used for the flow analysis of an axial-flow fan. A single-block H-type grid is generated by using the commercial preprocessor, GAMBIT.[11] To the

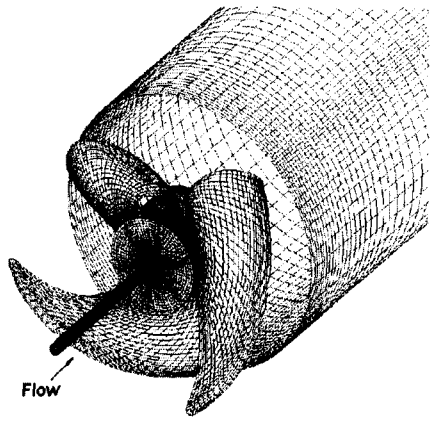

Fig. 3 Grid system.

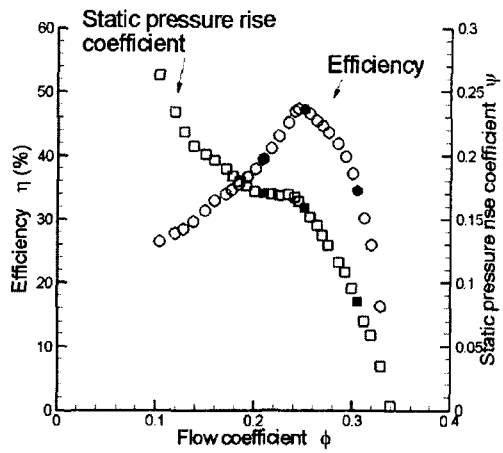

Fig. 4 Measured performance curve: ●, ■ represents the selected operating conditions.

author's experience, it was found that the stability and the convergence of the solution were greatly influenced by the number of grid cells and their distributions. Through the grid independency check, grid structure of 83 cells in the streamwise direction, 31 cells in the blade-to-blade direction, and 51 cells in the spanwise direction is optimally selected. Five cells in the spanwise direction are distributed between the blade tip and the casing wall with the near-wall clustering enough to capture the shear layer interaction that rules TLV trajectory. The first grid point from the nearest wall is located between $y^+=30$ and 60 to validate the use of the wall function.

4. Results

4.1 Performance curve

The overall performance curve is shown in Fig. 4. A flow coefficient (ϕ), a static pressure rise coefficient (Ψ), and a static efficiency (η) are defined as

$$\phi = Q/[U_t \pi(D_c^2 - D_h^2)/4] \quad (1)$$

$$\Psi = \Delta P_s/(\rho U_t^2/2) \quad (2)$$

$$\eta = Q \times \Delta P_s/L \quad (3)$$

where Q is the volume flow rate, ΔP_s is the static pressure rise, U_t is the blade tip speed, D_c is the casing diameter, D_h is the hub diameter, ρ is the density, and L is the shaft power. As shown in Fig. 4, the computation is conducted at three different conditions: small flow rate ($\phi=0.21$), peak efficiency ($\phi=0.25$), and large flow rate condition ($\phi=0.30$). Because the validity of the computed results at peak efficiency condition ($\phi=0.25$) was previously verified by comparing with LDV measurement data,[10] only the compared results at large flow rate condition ($\phi=0.30$) will be presented in the current study (see Figs. 6 and 9).

Figure 5 shows the static pressure distri-

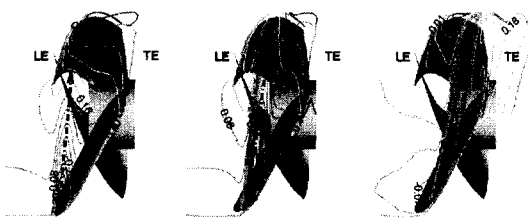

(a) $\phi=0.21$ (b) $\phi=0.25$ (c) $\phi=0.30$

Fig. 5 Static pressure coefficients on the casing (computation).

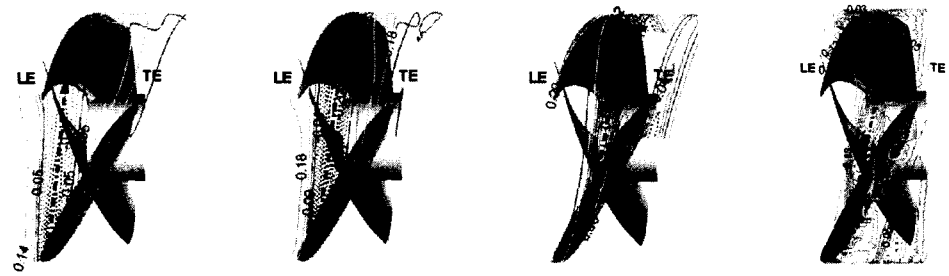

(a) ϕ=0.21 (comp.) (b) ϕ=0.25 (comp.) (c) ϕ=0.30 (comp.) (d) ϕ=0.30 (exp.)

Fig. 6 Contours of the normalized axial velocity component inside tip region (r/R_{tip}=1.004).

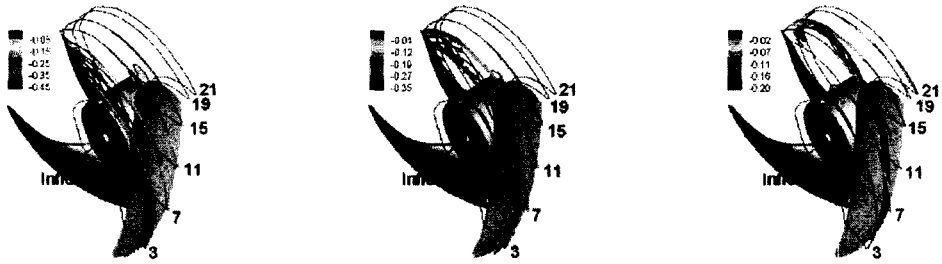

(a) ϕ=0.21 (b) ϕ=0.25 (c) ϕ=0.30

Fig. 7 Particle traces and the distribution of the reverse flow inside the blade passage (computation).

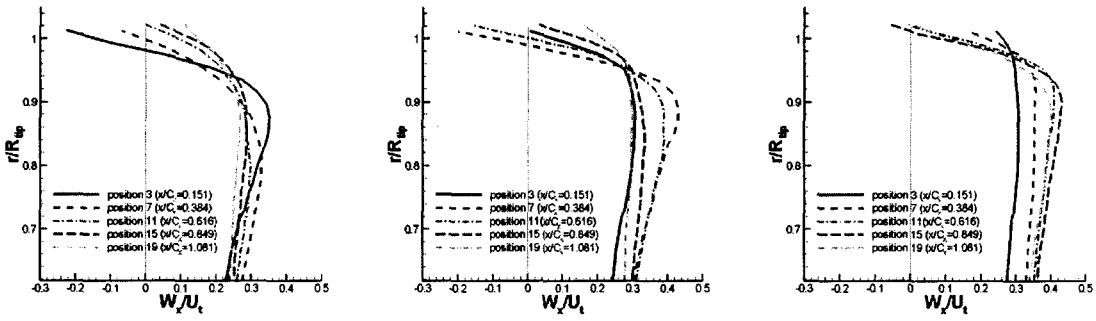

(a) ϕ=0.21 (b) ϕ=0.25 (c) ϕ=0.30

Fig. 8 Circumferentially mass-averaged axial velocity (computation).

bution on the casing. The static pressure coefficient is calculated from

$$C_{ps} = \frac{P - P_1}{\rho U_t^2/2} \tag{4}$$

where P_1 is the inlet static pressure.

The rolling-up of tip leakage flow is initiated near the position of the maximum static pressure difference (represented by the symbol □), and develops along the centerline of the pressure trough caused by the interaction of TLV with the casing wall (represented by a dotted line) within the blade passages. As the flow coefficient decreases (in other words, as the incidence or blade loading increases), the position of TLV initiation moves to the leading edge of the blade, that is, approximately 9%

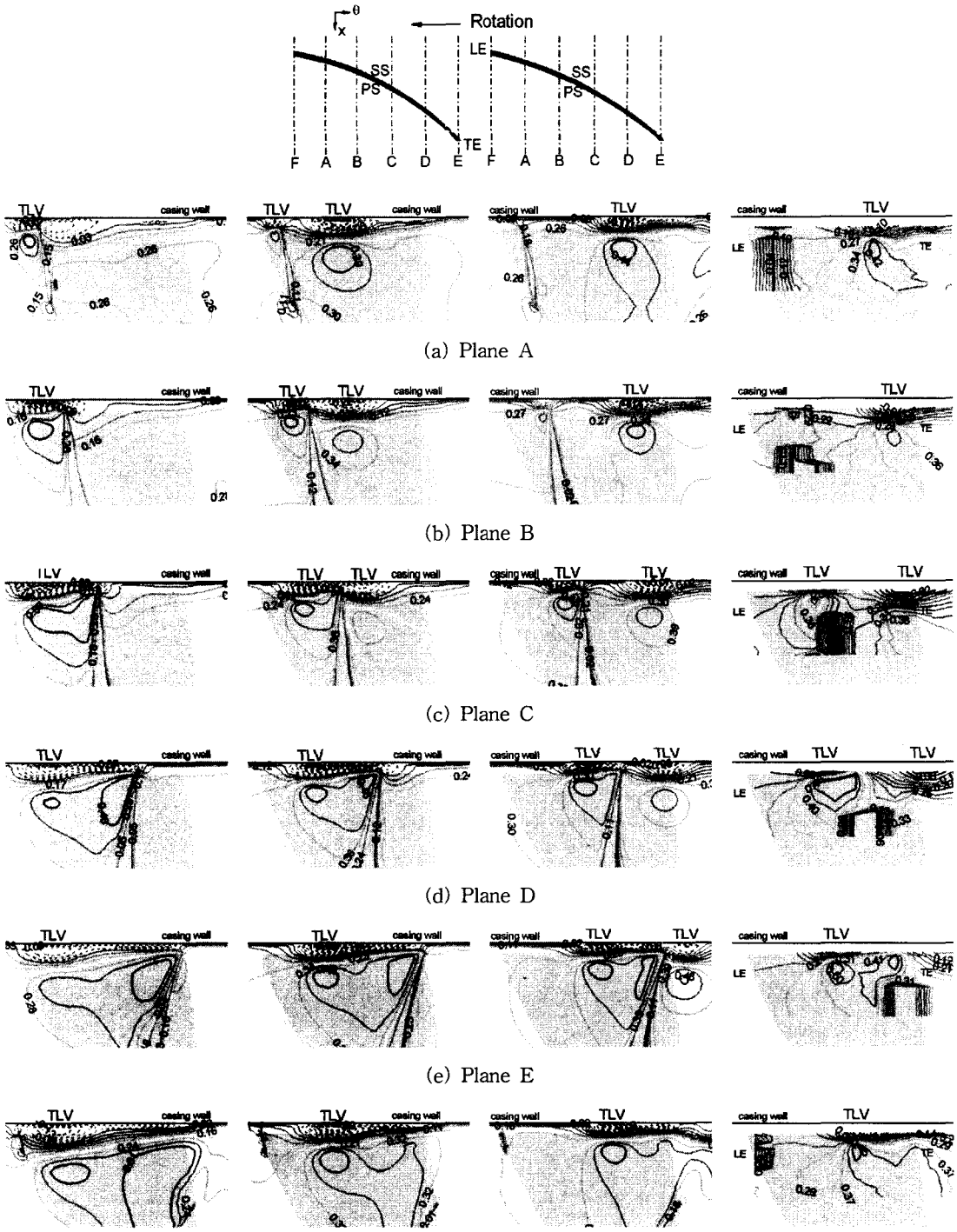

(a) Plane A

(b) Plane B

(c) Plane C

(d) Plane D

(e) Plane E

(f) Plane F

Fig. 9 Contours of the normalized axial velocity component at selected meridional planes (from the left column: ϕ=0.21 (comp.); ϕ=0.25 (comp.); ϕ=0.30 (comp.); ϕ=0.30 (exp.)).

axial tip chord of the blade from the leading edge for $\phi=0.21$, 12% for $\phi=0.25$, and 38% for $\phi=0.30$. As the blade loading increases, the trajectory of TLV center is more inclined toward the circumferential direction.

Figure 6 shows the distribution of an axial velocity normalized by the blade tip speed inside tip gap, which is located at $r/R_{tip}=1.004$. The regions with the negative axial velocity are represented by a dotted line in Fig. 6. This reverse flow results from the rolling-up of tip leakage flow and therefore it coincides with the pressure trough shown in Fig. 5.

At $\phi=0.21$ the reverse flow generated from near the leading edge of the blade suction side convects downstream with the nearly peripheral direction to the pressure side of the neighboring blade. As the flow coefficient increases, the angle between the locus of TLV and the blade suction side diminishes. At $\phi=0.30$ the predicted reverse flow region shows a reasonable agreement with the experimental one.

Figure 7 shows the formation of TLV and its development by both the distributions of the reversed flow and particle traces released inside tip gap. The particle traces are not constrained in the radial direction and therefore represent three-dimensional structure. Strong helical motion due to the roll-up of tip leakage flow extends to the pressure side of the adjacent blade. The generation position of the reversed flow, which is occurred due to the leakage jet and TLV near the casing, moves towards the leading edge, and its magnitude strengthens with blade loading increasing.

Figure 8 shows the circumferentially mass-averaged axial velocity at each cross-sectional plane shown in Fig. 2. At $\phi=0.21$ the magnitude of the reverse flow at position 3 is diminished with axial distance, and the velocity defect near the casing wall is gradually recovered. The flow acceleration near $r/R_{tip}=0.88$ is related with the blockage effect of TLV. As the blade loading decreases, the existing position of this flow acceleration moves downstream. For example, the high momentum region at $\phi=0.25$ is observed further downstream (position 7). At $\phi=0.30$ the existence of the negative axial velocity at position 19 gives a clue that TLV extends to the blade trailing edge.

Figure 9 shows the contours of the normalized axial velocity in six meridional planes denoted by planes 'A' through 'F'. Because of the beam reflection and the blockage on the optical laser, it is impossible to measure the velocity field near the blade and therefore the blank region exists there. The reverse flow region between the blade tip region and the casing, which are represented by a dotted line in Fig. 9, acts as a blockage on the through-flow. As a result, high momentum flux is observed below TLV.

At $\phi=0.25$ and 0.30, TLV located at the aft part of the blade is generated from the neighboring blade. At $\phi=0.21$ the TLV which initiates between plane A and F convects to the pressure side of the adjacent blade with little variation of axial position, and the magnitude of the reversed flow induced by TLV gradually diminishes. As shown in Fig. 5 (a), the fact that the pressure trough on the casing is not shown distinctly near the pressure side of the neigh-

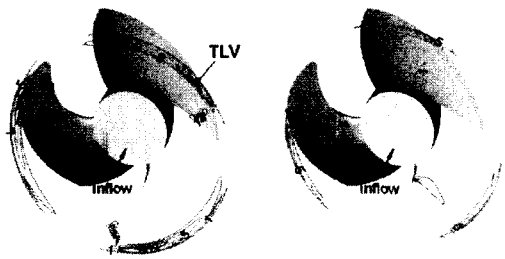

(a) Position 2 (b) Position 7

Fig. 10 Normalized streamwise vorticity distribution inside blade passage at $\phi=0.21$ (computation).

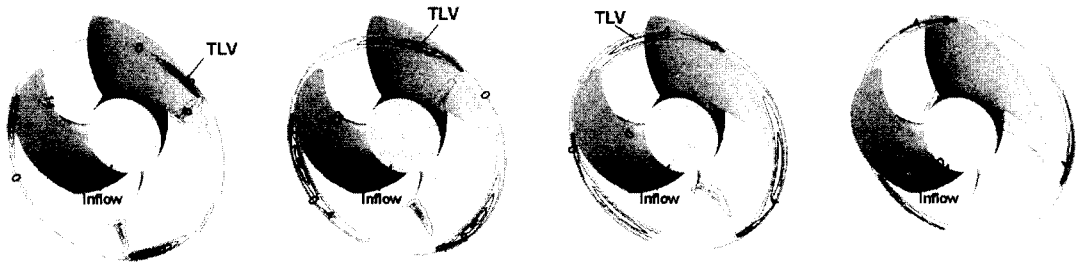

(a) Position 3 (b) Position 5 (c) Position 7 (d) Position 13

Fig. 11 Normalized streamwise vorticity distribution inside blade passage at $\phi=0.25$ (computation).

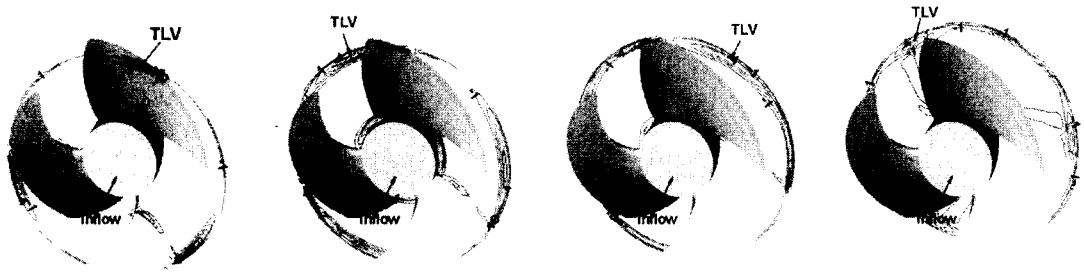

(a) Position 7 (b) Position 11 (c) Position 15 (d) Position 21

Fig. 12 Normalized streamwise vorticity distribution inside blade passage at $\phi=0.30$ (computation).

boring blade supports this explanation. As the blade loading decreases, TLV is generated from further downstream. At $\phi=0.30$ the predicted size and locus of TLV show a reasonable agreement with the measurement.

Figures 10 through 12 show the distribution of the normalized streamwise vorticity defined as

$$\omega_s = \frac{\vec{\omega} \cdot \vec{W}}{2\Omega |\vec{W}|} \tag{5}$$

where $\vec{\omega}$ is the absolute vorticity, $\vec{W}$ is the relative velocity vector, and Ω is the rotational speed of the blade. The negative value of vorticity indicates that TLV has a clockwise direction viewed from downstream. The streamwise vorticity has a large magnitude in the leakage jet and TLV region. As the blade loading increases, the streamwise vorticity decayed more rapidly due to the strong interaction with the through-flow and the casing boundary layer, and the diffusion of TLV by high turbulence. A distinct TLV is observed downstream of the blade trailing edge at $\phi=0.30$, but it is not observed at $\phi=0.21$ and 0.25.

Because the turbulence intensity is closely related with the generation of aero-acoustic noise, the distributions of turbulence intensity

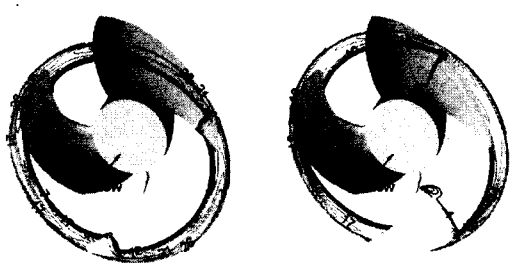

(a) Position 2 (b) Position 7

Fig. 13 Distributions of turbulence intensity inside blade passage at $\phi=0.21$ (computation).

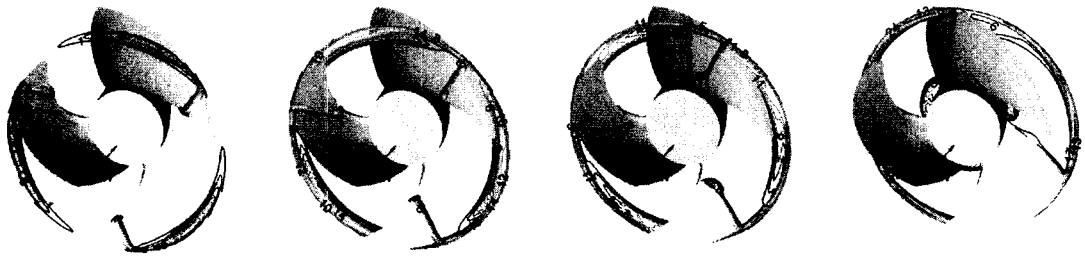

(a) Position 3 (b) Position 5 (c) Position 7 (d) Position 13

Fig. 14 Turbulence intensity distribution inside blade passage at $\phi=0.25$ (computation).

(a) Position 7 (b) Position 11 (c) Position 15 (d) Position 21

Fig. 15 Turbulence intensity distribution inside blade passage at $\phi=0.30$ (computation).

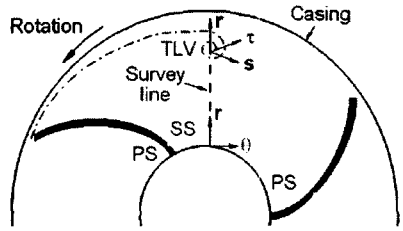

(a) Coordinate system based on the vortex center

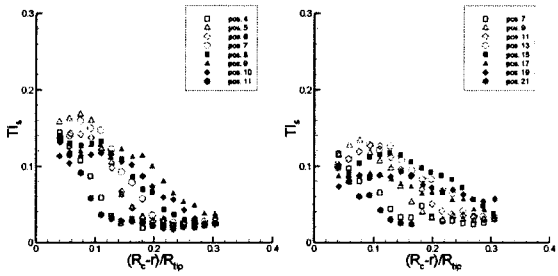

(b) Streamwise

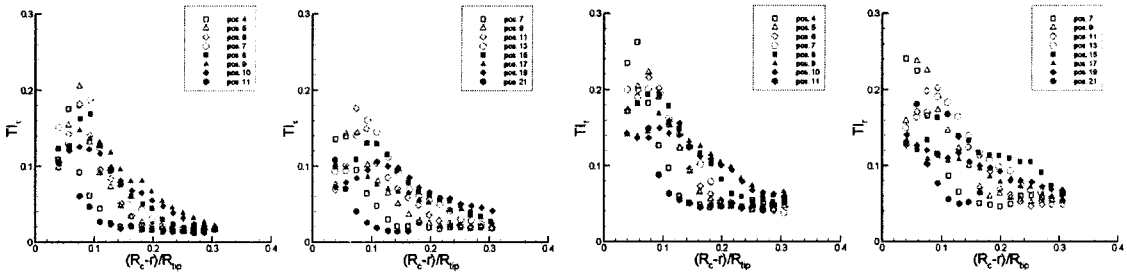

(c) Normal (d) Radial

Fig. 16 Turbulence intensity along the survey line (left; $\phi=0.25$, right; $\phi=0.30$)-measurement.

calculated with the normal stress components is shown in Figs. 13 through 15. The presented turbulence intensity is non-dimensionalized by the blade tip speed. The turbulence intensity has a large magnitude in the leakage jet and TLV region. Turbulence intensity increases, and high intensity region near the casing extends in the radially inward direction with the blade loading. The reason is that the casing boundary layer is thicker and the magnitude of tip leakage flow increases with the blade loading, and therefore the flow mixing through the interaction with the through-flow increases.

To investigate the detailed characteristics of TLV, the new coordinate system (s, τ, r) which passes through the center of TLV is defined in Fig. 16 (a). Here, s, τ, and r represents the streamwise, the normal, and the radial direction respectively.

Figures 16 (b) through 16 (d) show the turbulence intensity along the survey line in each direction. High turbulence intensity is measured inside TLV. It is the rotation effect and TLV that contribute significantly to the generation of the radial turbulence component near the tip region. As a consequence, turbulence intensity in the radial direction is much higher than that in the other directions. This anisotropic nature of the turbulent flow field inside TLV validates the use of the RSM for the quantitative prediction of TLV structure.

5. Conclusions

An experimental analysis using three-dimensional laser Doppler velocimetry (LDV) measurement and computational analysis using the Reynolds stress model of the commercial flow solver, FLUENT, are conducted to give a clear understanding of the effect of blade loading on the structure of tip leakage flow in a forward-swept axial-flow fan and the major conclusions could be summarized as follows:

(1) As the blade loading increased, the onset position of TLV moved upstream and the trajectory of TLV center was more inclined toward the circumferential direction.

(2) Because of the thicker casing boundary layer and the enhanced mixing between the through-flow and the leakage jet with the different flow direction, high turbulence intensity region near the casing extended in the radially inward direction, and the streamwise vorticity decayed more rapidly with blade loading increasing.

(3) A distinct TLV is observed downstream of the blade trailing edge at $\phi=0.30$, but it is not observed at $\phi=0.21$ and 0.25. In this way, the patterns of TLV were greatly influenced by the blade loading.

(4) In comparison with LDV measurement data, the computed results predicted the complex viscous flow patterns inside the tip region.

Acknowledgement

This work was supported by the Brain Korea 21 Project.

References

1. Lauchle, G. C., MacGillivray, J. R. and Swanson, D. C., 1997, Active control of axial-flow fan noise, J. Acoust. Soc. America, Vol. 101, pp. 341-349.
2. Quinlan, D. A. and Bent, D. A., 1998, High frequency noise generation in small axial flow fans, J. Sound Vibration, Vol. 218, pp. 177-204.
3. Wagner, J. H., Dring, R. P. and Joslyn, H. D., 1983, Axial compressor middle stage secondary flow study, NASA-3701.
4. Pandya, A. and Lakshminarayana, B., 1983, Investigation of the tip clearance flow inside and at the exit of a compressor rotor passage-Part I: mean velocity field, ASME J. Eng. Power, Vol. 105, pp. 1-12.

5. Myung, H. J. and Baek, J. H., 1999, Mean velocity characteristics behind a forward-swept axial-flow fan, JSME Int. J. (B), Vol. 42, pp. 476-488.
6. FLUENT, 2001, User's guide Ver. 6, Fluent Inc.
7. Myung, H. J., Baek, J. H., Rew, H. S. and Lee, I. S., 1999, Turbulence chracteristics of a leakage vortex in an axial-flow fan, Proc. of KFMA Meeting, Seoul, Korea, pp. 227-233.
8. Myung, H. J. and Baek, J. H., 1999, Measurement of the flow behind an axial-flow fan using three-dimensional LDV, Proc. of SAREK Meeting, Seoul, Korea, pp. 563-567.
9. Myung, H. J., Baek, J. H. and Lee, I. S., 2000, A study of the flows of an axial flow fan, Proc. 1st National Cong. Fluids Eng., Muju, Korea, pp. 667-670.
10. Lee, G. H., Myung, H. J. and Baek, J. H., 2003, Structure of tip leakage flow in a forward-swept axial-flow fan, Flow, Turbulence and Combustion, Vol. 70, pp. 241-265.
11. GAMBIT, 2001, User's guide Ver. 2, Fluent Inc.